

# Effect of Tungsten Trioxide Nanosheets Prepared under Low-energy State on Wood Surface Modification

Minglei Sun <sup>a,b</sup> and Kuiyan Song <sup>b,\*</sup>

Tungsten trioxide (WO<sub>3</sub>) nanosheets were deposited onto a wood surface by a solvothermal synthesis method using temperatures between 90 and 120 °C. These WO<sub>3</sub> nanosheets were used to improve the color, as well as to enhance the photochromic characteristics and ultraviolet aging resistance of the wood. The results indicate that the WO<sub>3</sub> nanosheets on the wood's surface were affected by the treatment temperature. The formed nanosheets included nanoparticles and rod-shaped structures, which are highly crystallized. Different structures were generated in the nanosheets, which affected their functionality. The modified wood not only exhibited photochromic phenomena when excited by ultraviolet radiation, but also demonstrated resistance against ultraviolet light aging.

*Keywords:* Tungsten trioxide; Wood modification; Phototropy; Ultraviolet aging resistance

*Contact information:* a: School of Design & Art, Shenyang Aerospace University, Shenyang 110136, PR China; b: Key Laboratory of Bio-Based Material Science and Technology of the Ministry of Education, Northeast Forestry University, Harbin 150040, PR China; \*Corresponding author: skuiyan@126.com

## INTRODUCTION

With the continuous increase in human demand, wood materials should be efficiently used to satisfy industrial development. Traditional uses for wood depend on its mechanical and physical attributes (Sun and Zhao 2018; Zhao *et al.* 2018a,b). Many investigators have investigated the modification of wood surfaces using nanomaterials. Generally, the modification of wood surfaces involves the use of inorganic (*e.g.*, ZnO and TiO<sub>2</sub>) nano-films fabricated using sol-gel and hydrothermal crystallization methods (Liu *et al.* 2013). These films bring some functional effects on wood materials in term of dimensional stability, mechanical strength, surface anticorrosion, anti-ultraviolet aging, super-hydrophobicity performance, and photocatalytic degradation of volatile organic compounds. (Li *et al.* 2010, 2013).

Tungsten trioxide (WO<sub>3</sub>) is an n-type semiconductor whose energy gap (approximately 2.7 eV) is smaller than that of TiO<sub>2</sub> (Waller *et al.* 2012). WO<sub>3</sub> is photostable to visible light energy and is widely used to develop electrochromic, photochromic, and photocatalytic materials, as well as sensors and lithium batteries (Zheng *et al.* 2011, 2012; Zhang *et al.* 2012; Liu *et al.* 2014; Jie *et al.* 2015). Jung *et al.* (2019) designed hybrid electrodes with solution-processable, flexible, and transparent processes by depositing a WO<sub>3</sub> buffer layer on silver nanowires. Gao *et al.* (2017) fabricated a visible-light activate Ag/WO<sub>3</sub>-wood system to produce negative oxygen ions. Even without visible light irradiation, the concentration of negative oxygen ions could stay at a high level. Dense layers of vertically oriented WO<sub>3</sub> crystals were grown on aluminum oxide as anodes for photoelectrochemical water oxidation (Qin *et al.* 2012). Vernardou *et al.* (2011) carried out a study on the growth of tungsten oxide on

microscope glass, which exhibited reversible electrochemical response and marked photocatalytic activity under solar illumination, degrading stearic acid by 52%. Three kind of tungsten oxide ( $\text{WO}_3$ ) thin films have been fabricated on glass with good photochromic properties (Ding *et al.* 2012).  $\text{WO}_3$  is widely synthesized on the matrixes of glass and metal. However, few studies have focused on the matrix of wood.  $\text{WO}_3$  could be used to modify wood surfaces so that they will exhibit metachromatic phenomena when exposed to visible light. In addition, a change in wood color can be stimulated by adjusting the light intensity. Hui *et al.* (2015) studied the hydrothermal synthesis of  $\text{WO}_3$  nanosheets on wood surfaces using sodium tungstate as the raw material; the investigators examined the photochromism and hydrophobicity of the formed nanosheets. In their study, the reaction temperatures for synthesis of  $\text{WO}_3$  nanosheets on a wood surface were 90 °C and 110 °C, while the reaction times were 12 h and 24 h, respectively. Nanosheets with desirable properties can be formed on wood surfaces; however, the synthesis methods used to form the nanosheets require high reaction temperatures and long reaction times. Hence, this study focus on a synthesis method to form  $\text{WO}_3$  nanosheets with various nanostructural characteristics using low temperatures and shorter reaction times (4 h and 6 h).

$\text{WO}_3$  nanosheets were fabricated on a wood surface using ethanol as the solvothermal medium. The compositional characteristics and chemical components of the nanosheets were characterized by morphological analyses (SEM and TEM), as well as chemical component analyses (EDS, XRD, and FTIR). The growth mechanism of the  $\text{WO}_3$  nanosheets is proposed. Moreover, the effect of synthesis temperature on the characteristics of the nanosheets (*e.g.*, color, photochromism, and ultraviolet aging resistance) was explored.

## EXPERIMENTAL

### Materials

Poplar wood samples with dimensions of 20 mm (*l*) × 20 mm (*w*) × 10 mm (*t*) were obtained from the Harbin Plywood Factory (Harbin, China). Prior to surface treatment, the wood samples were ultrasonically cleaned with ethanol for 30 min and then rinsed several times with distilled water. Subsequently, the cleaned wood samples were dried for 60 °C for 48 h in an oven. Afterward, the wood samples had a mean moisture content of 8.6%. Tungsten hexachloride ( $\text{WCl}_6$ ) (99.5%), absolute ethanol (99.7%), cetyl trimethyl ammonium bromide (99.0%), urea, and acetone (99.5%) were purchased from Tianjin Kernel Chemical Reagent Co., Ltd. (Tianjin, China). All chemical reagents were used as received, with no further purification.

### Methods

In this study, the wood surface was modified using a solvothermal synthesis method to form  $\text{WO}_3$  nanosheets. A set amount of tungsten hexachloride ( $\text{WCl}_6$ ) was dissolved in absolute ethanol to form a 0.06 M solution; the solution was stirred for 30 min at room temperature and then poured into a 150-mL stainless steel high-pressure hydrothermal reactor, with a Teflon® lining, that also contained the wood sample, until it reached 105 mL in volume. The reactor was sealed and heated in an oven for 4 h at a specified temperature (90 °C, 100 °C, 110 °C, or 120 °C). Afterward, the reactor was

removed from the oven and cooled to room temperature. This was the first heating process during the synthesis of nanosheets.

The cooled reactor was then opened. Next, 10 mL of 0.01 M cetyl trimethyl ammonium bromide (CTAB) solution (in water) and 5 mL of 0.01 M urea solution (in water) were added to the reactor. The total volume of the mixture in the reactor was 120 mL. The mixture was stirred for 30 min at room temperature. The reactor was then sealed and heated in an oven to the same temperature used in the first heating process (90 °C, 100 °C, 110 °C, or 120 °C) for 6 h; this was the second heating process. The mixture was then cooled to room temperature. The treated wood samples were cleaned with ethanol in an ultrasonic cleaner for 30 min; afterward, the wood samples were rinsed several times with deionized water. The rinsed samples were then placed in a vacuum drying oven (60 °C) for 24 h. The modified samples were labeled Fc1, Fc2, Fc3, or Fc4 depending on which solvothermal treatment temperature was used (90 °C, 100 °C, 110 °C, or 120 °C, respectively).

### Analysis of Modified Surface

The microstructural morphologies and chemical components of untreated and treated wood surfaces were examined using field-emission scanning electron microscopy (FE-SEM) (Model JSM-7500; JEOL; Tokyo, Japan) and X-ray energy dispersive spectroscopy (EDS) (Model X-Max<sup>N</sup>; Oxford Instruments, Oxford, UK). Because the wood samples were non-conducting, the wood surface was sputter-coated with gold. The WO<sub>3</sub> nanostructure was observed by transmission electron microscopy (TEM) (Model JSM-2100; JEOL; Tokyo, Japan), with an accelerating voltage of 200 kV. The crystal structure of the WO<sub>3</sub> nanolayer was characterized by X-ray diffraction (XRD) (Model D/max2200; Rigaku; Tokyo, Japan) using a voltage of 40 kV, a 2θ range of 10° to 70°, and a scanning rate of 4°/min. Fourier transform infrared spectrometry (FTIR) (Model Nicolet; Thermo Fisher Scientific; Waltham, MA) was used to characterize the functional groups on the modified wood surfaces. The samples were scanned from wavenumbers 700 to 4000 cm<sup>-1</sup>; 16 scans were performed at a resolution of 4 cm<sup>-1</sup>.

### Photochromism Test

The surface color of the modified wood surface was characterized with a spectrophotometer (Model CM-2300d; Konica Minolta; Tokyo, Japan). The measured color value represents the ground state (“A”) for the sample. Afterward, the wood sample was placed in an ultraviolet lamp box (Dongguan Guangkai Instrument Co., Ltd.; Dongguan, China). The wavelength and the power of the ultraviolet light source were 365 nm and 25 W, respectively. The distance between the ultraviolet light source and the surface of the specimen was set at 15 cm. Samples were exposed to ultraviolet light for 1 h; afterward, the color of the exposed surface was measured again using the spectrophotometer. This measured value represented the excitation state (“B”) for the sample. The chromatic distortion between “A” and “B” states was expressed by ΔE. After exposure to ultraviolet light, the samples were stored in the dark at room temperature for 24 h. After storage, the color of the samples was measured. This measured value represents the recovery state of color (“A<sub>1</sub>”) of the sample. Color measurements used the CIELAB coordinates. The quantity ΔE is defined as:

$$\Delta E = \sqrt{(\Delta L^*)^2 + (\Delta a^*)^2 + (\Delta b^*)^2} \quad (1)$$

where  $L^*$ ,  $a^*$ , and  $b^*$  are the CIELAB color coordinates.  $L^*$  is the lightness index, which ranges from 100 (white) to 0 (black). Positive values of the coordinate  $a^*$  denote red, whereas negative values denote green. Positive values of the coordinate  $b^*$  denote yellow, whereas negative values denote blue. The differences between the initial and final values of  $a^*$ ,  $b^*$ , and  $L^*$  are denoted  $\Delta a^*$ ,  $\Delta b^*$ , and  $\Delta L^*$ , respectively.

### Anti-Ultraviolet Aging Test

Test wood samples were placed in an ultraviolet light box and irradiated with 365 nm and 25 W radiation for 480 h to study the photochromism. After irradiation, the samples were stored in a dark room at room temperature for 24 h. After reaching the recovery state (“A<sub>1</sub>”) of photochromism, the sample color was measured by the spectrophotometer. The chromatic distortion in reference to the “A” state was calculated using Eq. (1). This measurement was used to characterize the anti-ultraviolet aging of the sample.

## RESULTS AND DISCUSSION

### EDS Elemental Analysis

Elements on the sample surface were characterized by EDS. The spectra of the surfaces of the samples after solvothermal treatment (Fc1 to Fc4) are shown in Fig. 1 and Table 1. All spectra contain one evident peak for Au at 2.2 keV and one peak for W at 1.8 keV. It is important to note that for the solvothermal temperature interval of 90 °C to 110 °C, the content of W increased as the reaction temperature increased. However, the content of C at the treated wood surfaces declined. The W content continuously increased as the temperature increased to 110 °C. The mass percentage (82.6%) and atomic percentage (25.7%) values were higher for 110 °C samples than those at the other conditions. As the solvothermal temperature increased, the kinetic energy in the solvent medium increased, causing more WO<sub>3</sub> to diffuse to the wood surface and crystallize. At 120 °C, the W content in the samples gradually declined, while the mass percentage and atomic percentage values decreased by 8.4%. However, the C content slightly increased. This indicates that high solvothermal temperature can increase the solution’s thermodynamic driving force. As the shear stress of the reaction medium increased at 120 °C, more WO<sub>3</sub> crystals were desorbed from the wood surface and returned to the solvent phase, which slowed the growth of the nanosheet. Hence, the W content on the wood surface decreased accordingly. No Cl was observed in any of the spectra; this indicates that all the WCl<sub>6</sub> was completely hydrolyzed to WO<sub>3</sub>.

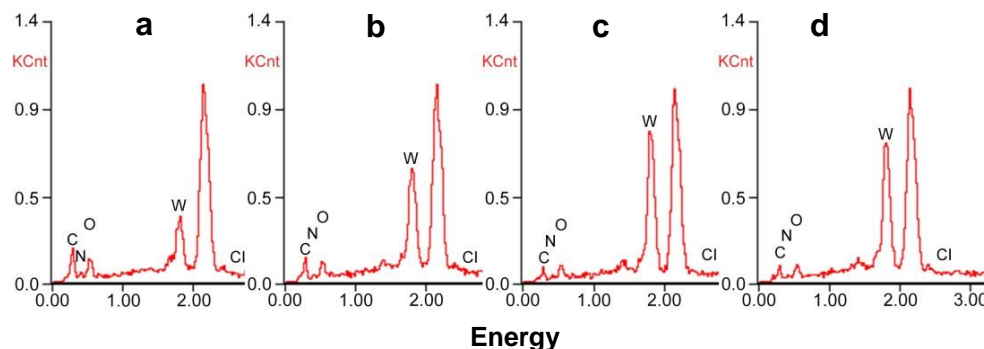


**Fig. 1.** EDS analysis of wood materials modified by WO<sub>3</sub>: (a) Fc1 (90 °C); (b) Fc2 (100 °C); (c) Fc3 (110 °C); and (d) Fc4 (120 °C)

**Table 1.** Contents of W and C in Wood Samples Modified by WO<sub>3</sub> Solvothermal Treatment

Specimens	W		C	
	Weight %	Atomic %	Weight %	Atomic %
Fc1 (90 °C)	36.76	4.03	33.96	56.96
Fc2 (100 °C)	64.56	11.61	19.39	53.39
Fc3 (110 °C)	82.57	25.66	9.12	43.37
Fc4 (120 °C)	74.26	17.21	14.04	49.81

### XRD Analysis of Crystalline Structure

The crystalline characteristics of W compounds in the nanosheet layer are given by the XRD spectra (Fig. 2). A comparative analysis of non-modified and modified wood samples (Fc1 to Fc4) was performed. The XRD spectra of all the samples had peaks at *ca.* 16° and 23°, which can be attributed to the crystalline cellulose contained in the wood (Shen *et al.* 2015). Some new diffraction peaks were observed for the treated samples (Fc1 to Fc4), at 13.7°, 23.7°, 28.4°, 34.1°, 49.5°, 56.1°, and 58.1°. These 2θ values correspond to the (110), (201), (200), (210), (220), (221), and (400) crystalline WO<sub>3</sub> planes, respectively. These diffraction planes are characteristic of the WO<sub>3</sub> hexagonal crystalline phase (Fu *et al.* 2015).

The intensity and the number of diffraction peaks changed as the solvothermal temperature changed, which indicates that the reaction temperature affected the WO<sub>3</sub> crystals on the wood surface. Relative crystallinities of the diffraction peaks corresponding to the (110), (210), (220), and (221) crystalline WO<sub>3</sub> planes increased from the Fc1 sample to the Fc3 sample (Fig. 2b), which indicates that high solvothermal temperature can increase the crystallinity and the crystal content of the WO<sub>3</sub> nanosheets formed at the wood surface (Zheng *et al.* 2013). When the solvothermal temperature was increased from 110 to 120 °C, the peak intensity and relative crystallinities were observed to decrease. This observation is consistent with the EDS analysis. Increasing the solvothermal temperature from 90 to 120 °C can facilitate the growth of WO<sub>3</sub> crystals on the wood surface. However, further increases in solvothermal temperature (>110 °C) increased the medium shear stress, which impeded crystal growth at the phase interface. Consequently, the diffraction peak intensities for the WO<sub>3</sub> crystals were lower.

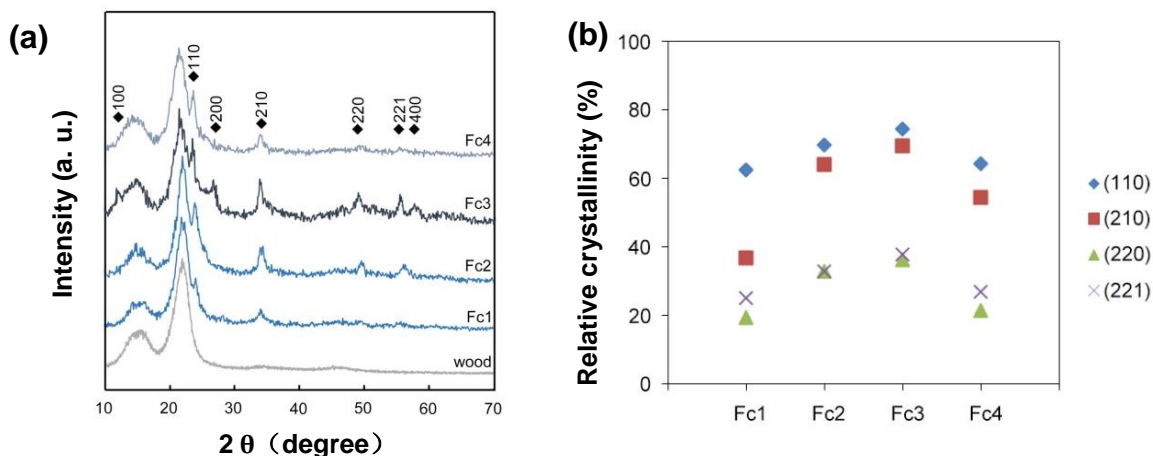


**Fig. 2.** XRD pattern of a non-modified wood sample and treated wood samples (a); and relative crystallinity of selected peaks of treated wood samples (b)

### FTIR Analysis of Functional Groups

The FTIR spectra (Fig. 3) show that the surfaces of the modified wood samples had enhanced peaks at 3335 and 810  $\text{cm}^{-1}$ , but had weakened peaks at 1460 and 1506  $\text{cm}^{-1}$ . The 3335  $\text{cm}^{-1}$  peak can be attributed to H-O stretching with hydroxyl groups (Lesar *et al.* 2013). This absorption peak is intensified after solvothermal surface treatment; this may be attributed to the increase in hydrogen bonds between the  $\text{WO}_3$  crystals and the hydroxyl groups on the wood surface. The absorption peaks at 1460 and 1506  $\text{cm}^{-1}$  can be assigned to the lignin in the wood (Pandey 1997). The intensities of these peaks decreased for the modified woods, which indicates some degradation of wood components during solvothermal treatment. Nevertheless, the absorption peak at 810  $\text{cm}^{-1}$  for Fc3 can be assigned to the stretching and bending vibration of the O-W-O in the  $\text{WO}_3$  crystals (Bai *et al.* 2012). This absorption peak provides experimental evidence for the presence of crystalline  $\text{WO}_3$  structures at the wood surface.

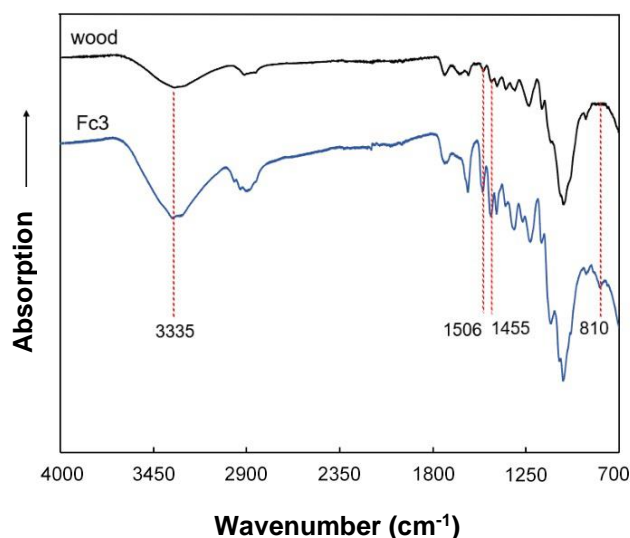


Fig. 3. FTIR spectra of non-modified wood and sample Fc3

### SEM Analysis

SEM images of Fc1 (90 °C), Fc2 (100 °C), Fc3 (110 °C), Fc4 (120 °C), and non-modified wood are shown in Fig. 4. It can be seen from the SEM images of Fc1 (Fig. 4-a2) that the wood surface contained a thin film of amorphous  $\text{WO}_3$ , accompanied by some projecting nanoparticles on the surface. In Fig. 4-b2, the crystalline particles on the Fc2 surface are rod-shaped, with clear spaces between them. The mean diameter and length of the crystalline particles were approximately 120 nm and 750 nm, respectively. These particles overlapped, and the thickness of the overlapping layer was relatively uniform, at approximately 410 nm. A layered structure was evident on the surface. Compared with Fc1 and Fc2, the morphology of crystal growth on Fc3 (Fig. 4-c2) was denser because the thermodynamic driving force was higher. Moreover, the size of the nanoparticles increased slightly, and the space among the nanoparticles decreased. This led to a smoother crystal layer surface. According to the morphology in Fig.4-c1, a smooth crystal modification layer formed along the edges of the wood cell wall. The morphology of sample Fc4 is shown in Fig. 4-d2; the space among nanoparticles disappeared, forming a relatively smooth modification layer. Influenced by the shear stress of the solution, the modification layer thickness was decreased to some extent

compared with the modification layer thickness for samples modified at 110 °C, and some spherical protuberances developed. Additionally, full and uniform  $\text{WO}_3$  layers formed along the edges of the wood cell wall.

Semi-spherical or cylindrical aggregates were observed at the wood surface. This is attributed to the uneven microstructure of wood (Fig. 4-e1).  $\text{WO}_3$  crystal growth is influenced by the adsorption forces on the wood surface and by the shear stresses of the solvent. Semi-spherical or cylindrical aggregate crystal structures will appear at a rough wood surface.

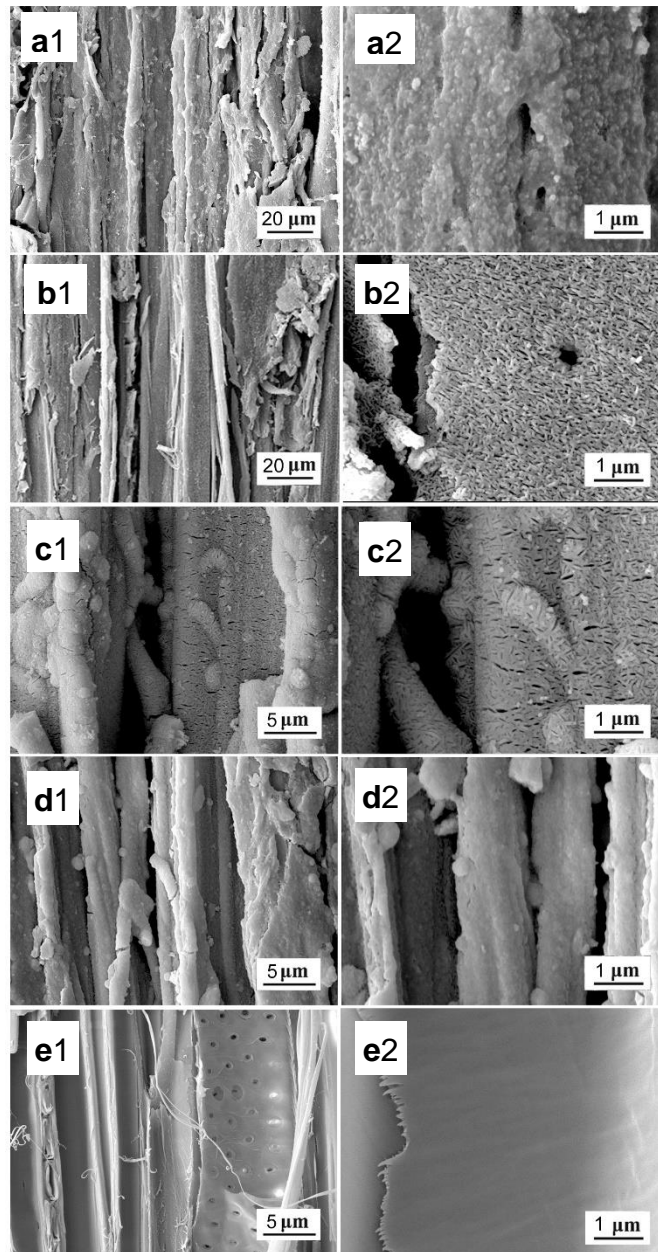


**Fig. 4.** SEM images of Fc1 to Fc4 treated wood (a-d), and non-modified wood (e), at low magnification for a1, b1, c1, d1, and e1; and at high magnification for a2, b2, c2, d2, and e2

The crystal lattice and microstructure of wood surfaces modified by  $\text{WO}_3$  were further analyzed according to the TEM images of Fc4. It can be seen from Fig. 5a that in the light field image of TEM, the maximum length of the irregular profile of the  $\text{WO}_3$  nanoparticle reached approximately 800 nm. From the local magnification of the  $\text{WO}_3$  nanoparticle, reticulate crystal structures (crystal lattice of  $\text{WO}_3$ ) can be seen (Fig. 5b). These results suggest that  $\text{WO}_3$  can form dense crystal structures on wood surfaces under heating conditions, thus improving the surface functions of wood materials.

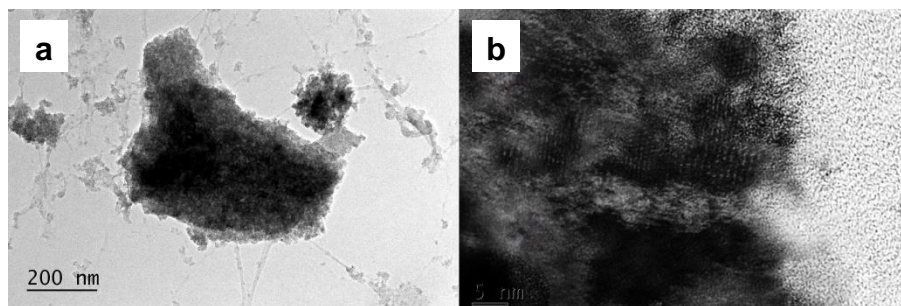
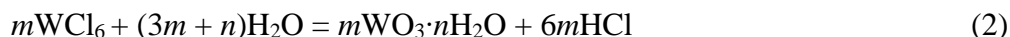


Fig. 5. TEM images of Fc4 (a: light field image; and b: local magnification)

### Surface Modification Mechanism of $\text{WO}_3$

The surface of wood is mostly composed of cell wall substances and full of polar groups, such as  $-\text{OH}$  and  $-\text{COOH}$ . During the first heating of the solvothermal process, the  $\text{WCl}_6$  particles that are dissolved in the ethanol medium are hydrolyzed (Eq. 2). Hydrolysis generates hydrated tungstate particles ( $m\text{WO}_3 \cdot n\text{H}_2\text{O}$ ), which are subsequently dehydrated by heat to  $\text{WO}_3$  (Eq. 3).  $\text{WO}_3$  structures bond with polar groups on the wood cell wall, which become the *in-situ* points for subsequent growth of crystalline  $\text{WO}_3$ . During the second heating of the solvothermal process, the added active agent causes the abundant  $\text{WCl}_6$  to complete hydrolysis in the solution. This provides  $\text{WO}_3$  particles for subsequent growth of the crystals on the wood surface. Moreover, the resulting hydrolysis product,  $\text{HCl}$ , acidified the reaction medium, which further promoted adsorption and crystal growth of  $\text{WO}_3$  at the wood surface.



The growth of crystalline  $\text{WO}_3$  on wood surfaces involves the transformation of crystal particles among the environmental phase, interface phase, and crystal phase. The thermodynamic driving force provides an essential transport force for  $\text{WO}_3$  particles from the environmental phase to the interface phase and crystal phase. Some of these  $\text{WO}_3$  particles are adsorbed on the polar wood surface, and the others are desorbed from the interface phase and return to the environmental phase. The  $\text{WO}_3$  content at the wood surface increased as the temperature increased from 90 to 110 °C. The amount of adsorbed  $\text{WO}_3$  particles increased with increasing temperature. At 120 °C, the reaction medium had higher kinetic energy, which increased the shear stress of the fluid at the interface to the point where  $\text{WO}_3$  particles could not adsorb onto the solid surface. The adsorption-desorption process shifts to desorption (Fig. 6), which slowed the growth of crystals at the wood surface. This reduced the amount of W that the wood contained when it was treated at 120 °C. The higher kinetic energy of the reaction medium at 120 °C also reduced the relative crystallinity of  $\text{WO}_3$ .

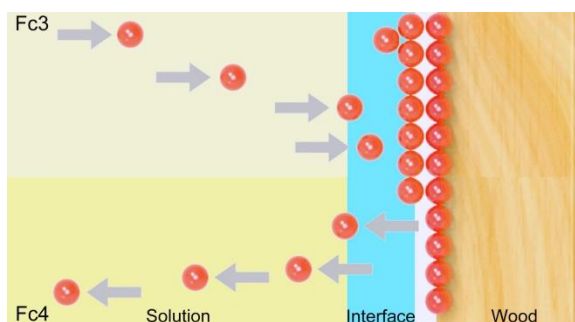


**Fig. 6.** Proposed solvothermal mechanism for the growth of  $\text{WO}_3$  crystals on the wood surface

### Color and Photochromatic Properties

The color changes in the wood samples after various  $\text{WO}_3$  solvothermal treatments are shown in Fig. 7. As the treatment temperature increased, the surface color darkened because of the degradation of wood components. Moreover, the  $\text{WO}_3$  acted like a wood staining agent.



**Fig. 7.** (A) Color and (B) photochromism of non-modified and  $\text{WO}_3$ -modified wood samples

The chromatic distortion (or aberration) of the test samples before and after ultraviolet irradiation was evaluated using Eq. 1. The  $\Delta E^*$  value of the non-modified wood was 1.8 after 1 h of ultraviolet irradiation; this suggests that the unmodified wood had weak color distortion. This minor change in wood color is caused by the aging of wood components with ultraviolet irradiation. All solvothermal-treated wood samples exhibited color distortions when exposed to ultraviolet irradiation (Fig. 8). The average of the  $\Delta E^*$  values for the treated wood samples was 17.6. The color distortion increased when the treatment temperature was increased from 90 to 110 °C. The  $\Delta E^*$  of Fc3 (110 °C) after ultraviolet irradiation was 20.2; the  $\Delta E^*$  for Fc4 (120 °C) was lower than the  $\Delta E^*$  of Fc3 (110 °C). It can be seen that the change of  $\Delta E^*$  (Fig. 8) and the relative crystallinity (Fig. 2b) exhibited the same trend. These color distortions were directly correlated with the crystallization of  $\text{WO}_3$  in the nanosheets.

Changes to  $\Delta a^*$  (*i.e.*, green to red) were not appreciable in all the wood samples. Changes to  $\Delta b^*$  (*i.e.*, blue to yellow) after ultraviolet irradiation for the treated wood samples were noticeable: the  $\Delta b^*$  offset was toward blue. This is directly related to the transformation from yellow to blue by thin  $\text{WO}_3$  nanosheets when excited by ultraviolet irradiation (Ng *et al.* 2014). The lightness differences ( $\Delta L^*$ ) of Fc1 and Fc4 samples were

not appreciable, whereas the  $\Delta L^*$  values for Fc2 and Fc3 were relatively high (11.8 and 12.7, respectively).

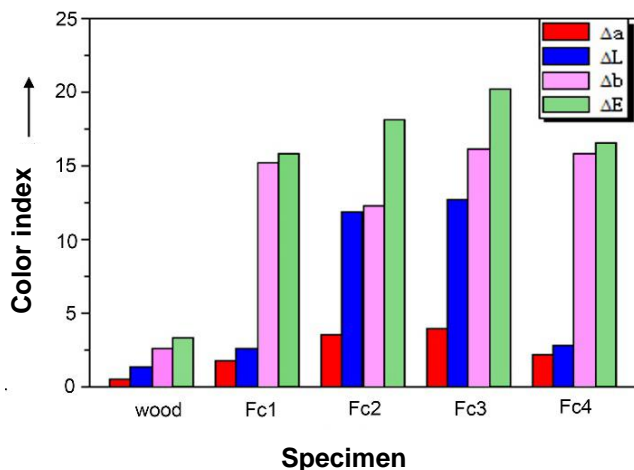


**Fig. 8.** Color distortions (measured as changes to the color indices) of the solvothermal-treated samples after 1 h of ultraviolet irradiation

The photochromism caused by  $\text{WO}_3$  is reversible. In separate experiments, samples were stored in a dark room at room temperature for 24 h after ultraviolet light exposure. The recovery color of the sample (“A1”) at room temperature was tested and compared with the color at ground state A (sample color before the photochromatic test). The chromatic distortion between these two states was calculated; this value represents how much of the sample’s original color is recovered ( $\Delta E_A$ ). When  $\Delta E_A$  is small, the color deviation is smaller. The  $\Delta E_A$  of the non-modified wood was 1.8, which indicates that the color deviation was small but not completely irreversible. Such irreversible color distortion is caused by the degradation of wood constituents upon ultraviolet irradiation. The  $\Delta E_A$  values for samples Fc1 to Fc4 ranged between 0.22 and 1.31, which indicates that most of the color distortion caused by ultraviolet irradiation was reversed. This shows that the  $\text{WO}_3$  nanosheets on the wood surface protected it from ultraviolet light.

### Anti-Ultraviolet Aging Performance

The chromatic distortions of the samples when exposed to ultraviolet radiation for a long time are shown in Fig. 9. The color of the non-modified wood was appreciably altered after 480 h of irradiation ( $\Delta E_0 = 21.7$ ). The chromatic distortion increased quickly during the first 200 h, and more particularly during the first 48 h. The rate of chromatic distortion remained invariable from 200 to 480 h. However, chromatic distortion of the non-modified wood after ultraviolet aging changed greatly, indicating serious degradation of non-modified wood components after ultraviolet aging. The  $\Delta E$  values of all modified wood samples were lower than 5 after the ultraviolet aging test. This observation indicates that all the  $\text{WO}_3$ -modified wood samples had a certain resistance to ultraviolet light aging. The  $\Delta E_1$  value of Fc1 was the highest (4.1), whereas the  $\Delta E_1$  value of Fc3 was the lowest ( $< 2.2$ ). The  $\Delta E$  value of Fc3 was low, which reflected the resistance imparted by the solvothermal treatment to ultraviolet light aging. This is related to the  $\text{WO}_3$  nanosheets formed, the degree of crystal growth in these layers, and the nanostructural characteristics composing these layers. It was revealed that the higher the degree of crystallinity of  $\text{WO}_3$ , the better was the anti-ultraviolet aging performance of

the surface. The nanosheets can absorb and scatter ultraviolet light, which can effectively protect the wood base from ultraviolet aging.

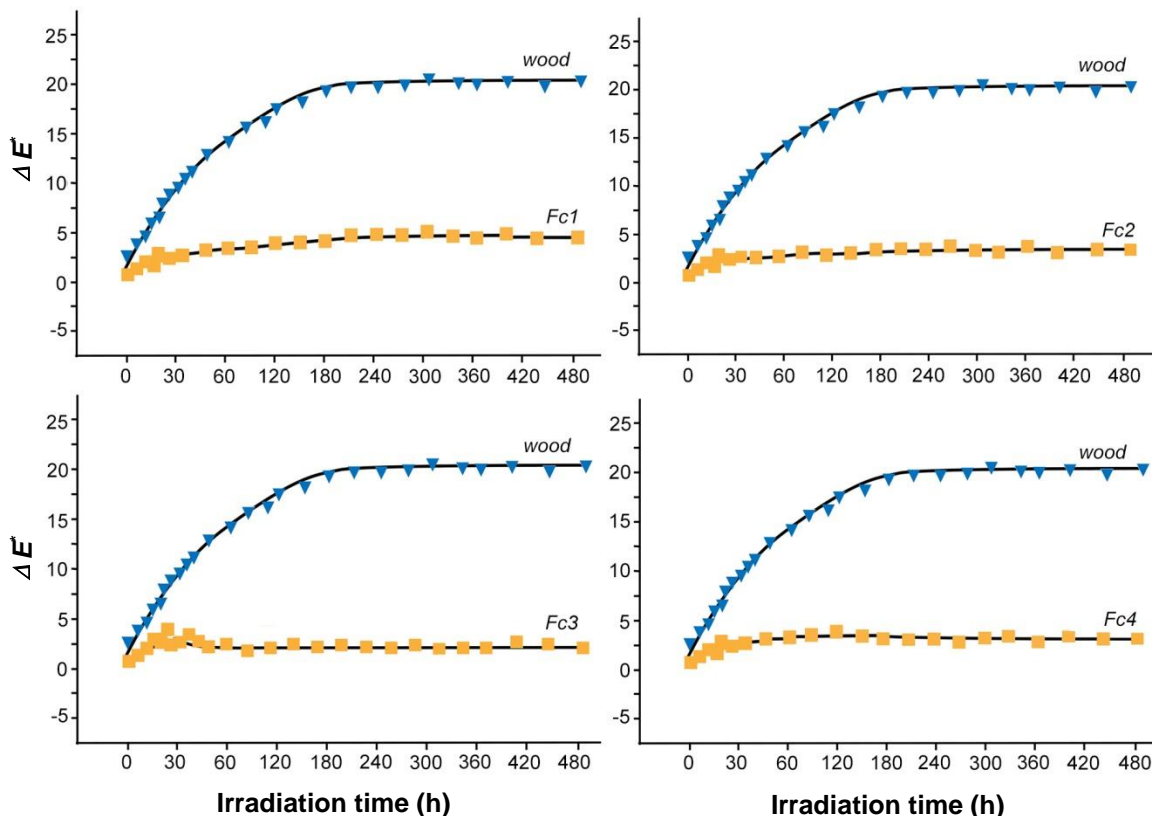


**Fig. 9.** Chromatic distortion caused by ultraviolet aging of non-modified and  $\text{WO}_3$ -modified wood samples as measured by changes to the color indices

## CONCLUSIONS

1. Wood surfaces were modified by the deposition of  $\text{WO}_3$  nanosheets during low-temperature solvothermal treatment using  $\text{WCl}_6$  as a precursor. Such modification stains the wood surface, as well as imparting photochromatic properties and ultraviolet light aging resistance to the surface.
2. Chemical and morphological analyses of the modified woods were performed. Results indicate that the W content in the modified wood samples increased and that a crystalline  $\text{WO}_3$  structure formed on the surface. These nanosheets on the surface have microstructural characteristics that depend on the solvothermal treatment temperature.
3.  $\text{WO}_3$  crystal growth was optimum when the solvothermal treatment was conducted at or below  $110\text{ }^\circ\text{C}$ . The wood sample treated at  $110\text{ }^\circ\text{C}$  (Fc3) had the best physical characteristics of all the conditions examined. Photochromatic characteristics and ultraviolet aging resistances of the wood surfaces were appreciably improved by solvothermal treatment.

## ACKNOWLEDGMENTS

The authors are grateful for the support of the National Science Foundation of China (No. 31770592).

## REFERENCES CITED

- Bai, S., Zhang, K., Luo, R., Li, D., Chen, A., and Liu, C. C. (2012). "Low-temperature hydrothermal synthesis of WO<sub>3</sub> nanorods and their sensing," *J. Mater. Chem.* 22, 12643-12450. DOI: 10.1039/C2JM30997A
- Ding, D., Shen, Y., Ouyang, Y., and Li, Z. (2012). "Hydrothermal deposition and photochromic performances of three kinds of hierarchical structure arrays of WO<sub>3</sub> thin films," *Thin Solid Films* 520, 7164-7168. DOI: 10.1016/j.tsf.2012.08.003
- Fu, L., Cai, W., Wang, A., and Zheng, Y. (2015). "Photocatalytic hydrogenation of nitrobenzene to aniline over tungsten oxide-silver nanowires," *Mater. Lett.* 142(12), 201-203. DOI: 10.1016/j.matlet.2014.12.021
- Gao, L. K., Gan, W. T., Cao, G. L., Zhan, X. X., Qiang, T. G., and Li, J. (2017). "Visible-light activate Ag/WO<sub>3</sub> films based on wood with enhanced negative oxygen ions production properties," *Appl. Surf. Sci.* 425, 889-895. DOI: 10.1016/j.apsusc.2017.06.327
- Hui, B., Li, Y., Huang, Q., Li, G., Li, J., Cai, L., and Yu, H. (2015). "Fabrication of smart coatings based on wood substrates with photoresponsive behavior and hydrophobic performance," *Mater. Design* 84, 277-284. DOI: 10.1016/j.matdes.2015.06.125
- Jie, X., Zeng, D., Zhang, J., Xu, K., Wu, J., Zhu, B., and Xie, C. (2015). "Graphene-wrapped WO<sub>3</sub> nanospheres with room-temperature NO<sub>2</sub> sensing induced by interface charge transfer," *Sensor. Actuat. B-Chem.* 220, 201-209. DOI: 10.1016/j.snb.2015.05.047
- Jung, S. G., Shim, Y. S., Park, C. H., Park, Y. W., and Ju, B. K. (2019). "Solution processable, flexible, and transparent hybrid electrodes using tungsten oxide buffer layer on silver nanowires," *J Nanosci. Nanotech.* 19(10), 6197-6201. DOI: 10.1166/jnn.2019.17012
- Lesar, B., Humar, M., Kamke, F. A., and Kutnar, A. (2013). "Influence of the thermo-hydro-mechanical treatments of wood on the performance against wood-degrading fungi," *Wood Sci. Technol.* 47(5), 977-992. DOI: 10.1007/s00226-013-0553-8
- Li, J., Yu, H., Sun, Q., Liu, Y., and Cui, Y. (2010). "Growth of TiO<sub>2</sub> coating on wood surface using controlled hydrothermal method at low temperatures," *Appl. Surf. Sci.* 256(16), 5046-5050. DOI: 10.1016/j.apsusc.2010.03.053
- Liu, J., Xu, Q., Shi, F., Liu, S., Luo, J., Bao, L., and Feng, X. (2014). "Dispersion of Cs<sub>0.33</sub>WO<sub>3</sub> particles for preparing its coatings with higher near infrared shielding properties," *Appl. Surf. Sci.* 309, 175-180. DOI: 10.1016/j.apsusc.2014.05.005
- Liu, Y., Fu, Y., Yu, H., and Liu, Y. (2013). "Process of *in situ* forming well-aligned zinc oxide nanorod arrays on wood substrate using a two-step bottom-up method," *J. Colloid Interf. Sci.* 407, 116-121. DOI: 10.1016/j.jcis.2013.06.043
- Ng, C. Y., Razak, K. A., and Lockman, Z. (2014). "WO<sub>3</sub> nanorods prepared by low-temperature seeded growth hydrothermal reaction," *J. Alloy. Compd.* 588, 585-591. DOI: 10.1016/j.jallcom.2013.11.096

- Pandey, K. K. (1997). "A study of chemical structure of soft and hardwood and polymers by FTIR spectroscopy," *J. Appl. Polym. Sci.* 71(12), 1969-1975. DOI: 10.1002/(SICI)1097-4628(19990321)71:12<1969::AID-APP6>3.0.CO;2-D
- Qin, D. D., Tao, C. L., Friesen, S. A., Wang, T. H., Varghese, O. K., Bao, N. Z., Yang, Z. Y., Mallouk, T. E., and Grimes, C. A. (2012). "Dense layers of vertically oriented WO<sub>3</sub> crystals as anodes for photoelectrochemical water oxidation," *Chem. Commun* 48, 729-731.
- Shen, Y., Yan, P., Yang, Y., and Hu, F. (2015). "Hydrothermal synthesis and studies on photochromic properties of Al doped WO<sub>3</sub> powder," *J. Alloy. Compd.* 629, 27-31. DOI: 10.1016/j.jallcom.2014.11.218
- Sun, S., and Zhao, Z. (2018). "Influence of acid on the curing process of tannin-sucrose adhesives," *BioResources* 13(4), 7683-7697. DOI: 10.15376/biores.13.4.7683-7697
- Vernardou, D., Drosos, H., Spanakis, E., Koudoumas, E., Savvakis, C., and Katsarakis, N. (2011). "Electrochemical and photocatalytic properties of WO<sub>3</sub> coatings grown at low temperatures," *J. Mater. Chem.* 21, 513-517. DOI: 10.1039/C0JM02413A
- Waller, M. R., Townsend, T. K., Zhao, J., Sabio E. M., Chamousis, R. L., Browning, N. D., and Osterloh, F. E. (2012). "Single-crystal tungsten oxide nanosheets: Photochemical water oxidation in the quantum confinement regime," *Chem. Mater.* 24(4), 698-704. DOI: 10.1021/cm203293j
- Zhang, H., Liu, T., Huang, L., Guo, W., Liu, D., and Zeng, W. (2012). "Hydrothermal synthesis of assembled sphere-like WO<sub>3</sub> architectures and their gas-sensing properties," *Physica E* 44(7-8), 1467-1472. DOI: 10.1016/j.physe.2012.03.013
- Zhao, Z., Hayashi, S., Xu, W., Wu, Z., Tanaka, S., Sun, S., Zhang, M., Kanayama, K., and Umemura, K. (2018a). "A novel eco-friendly wood adhesive composed by sucrose and ammonium dihydrogen phosphate," *Polymer* 10(6), 1251. DOI: <https://doi.org/10.3390/polym10111251>
- Zhao, Z., Miao, Y., Yang, Z., Wang, H., Sang, R., Fu, Y., Huang, C., Wu, Z., Zhang, M., Sun, S., *et al.* (2018b). "Effects of sulfuric acid on the curing behavior and bonding performance of tannin-sucrose adhesive," *Polymer* 10(11), 651. DOI: 10.3390/polym10060651
- Zheng, F., Zhang, M., and Guo, M. (2013). "Controllable preparation of WO<sub>3</sub> nanorod arrays by hydrothermal method," *Thin Solid Films* 534, 45-53. DOI: 10.1016/j.tsf.2013.01.102
- Zheng, H., Ou, J. Z., Strano, M. S., Kaner, R. B., Mitchell, A., and Kalantar-Zadeh, K. (2011). "Nanostructured tungsten oxide – Properties, synthesis, and applications," *Adv. Funct. Mater.* 21(12), 2175-2196. DOI: 10.1002/adfm.201002477

Article submitted: April 2, 2019; Peer review completed: July 6, 2019; Revised version received: September 22, 2019; Accepted: September 23, 2019; Published: October 1, 2019.

DOI: 10.15376/biores.14.4.9146-9158